



Complexity and information measures in planar characterization of chaos and noise

Hui Xiong · Pengjian Shang · Jiayi He ·
Yali Zhang

Received: 21 September 2019 / Accepted: 27 February 2020 / Published online: 11 March 2020
© Springer Nature B.V. 2020

Abstract In this work, we present a comprehensive assessment of the Fisher information measure and statistical complexity measures based on Euclidean distance, Wootters distance and Jensen–Shannon divergence, regarding their abilities to (planar-) distinguish between/among (1) chaos and periodicity; (2) different degrees of periodicities; (3) different chaotic regimes; and (4) chaos and noise, and characterize delay dynamics. The Bandt–Pompe approach is used to build up the probability space to generate the entropy-complexity/information plane. The effect of embedding parameters on the evaluation is also considered. Within this framework, complexity measures based on the Wootters distance and Jensen–Shannon divergence are superior to the Fisher information measure in capturing subtle details of chaotic dynamics. The Fisher information measure shows advantages in robustness to additive noises and in planar-behavior representation of chaos and noise. Moreover, all measures are able to properly characterize the intrinsic delay dynamics of chaotic and stochastic systems. Nevertheless, the complexity measure based on the Euclidean distance is not valid by definition, thus, not applicable at any cases.

Keywords Entropy-complexity plane · Fisher information measure · Statistical complexity · Bandt–Pompe approach · Chaos · Stochastic process · Time delay

1 Introduction

It is well acknowledged that there are three main types of complexity parameters, namely entropy [1, 2], fractal dimension [3, 4] and Lyapunov exponent (LE) [5]. These quantities provide a set of often-used and well-understood tools for the detection and quantification of various kinds of deterministic chaos of dynamical systems [6, 7]. Among them, Shannon’s entropy has been productively used as a measure of degree of randomness or unpredictability since it was proposed [2]. Moreover, many measures derived from Shannon’s entropy have been most widely adopted to characterize and quantify the complexity of dynamical systems, including topological entropy that measures the exponential growth rate of distinguishable orbits of the system [8], Kolmogorov–Sinai entropy that measures the complexity and chaos of the motion taking place in a dynamical system [9], permutation entropy that behaves similar to the LE [10], to name a few. Thereafter, the utilization of measures of complexity based on entropies has attracted lots of researchers from various fields, such as physiology [11–13], art [14], and machine learning [15–17].

H. Xiong (✉) · P. Shang (✉) · J. He · Y. Zhang
Department of Mathematics, School of Science,
Beijing Jiaotong University, Beijing 100044,
People’s Republic of China
e-mail: xionghui@bjtu.edu.cn

P. Shang
e-mail: pjshang@bjtu.edu.cn

The quantitative characterization of complexity has received considerable attention; however, there is no universal agreement. Generally, the complexity measures can be classified into three categories [18]: (i) complexity grows with disorder; (ii) complexity vanishes either at complete disorder or at complete order and has a maximum at certain intermediate stage; and (iii) complexity grows with order. Among them, the second type of complexity has a large number of supporters. It was pointed out that complexity is represented by a mixture of order and disorder rather than defined in terms of just order or regularity [19]. Complete periodic or random process does not contain any non-trivial structures. Following it, a statistical complexity measure incorporates two essential ingredients: entropy and disequilibrium in probability space, with the form $C = Q \cdot H$. The entropy H is usually referred to the information entropy, such as Shannon entropy and its generalization Tsallis or Rényi entropy [20]. The disequilibrium measures Q based on the Euclidean distance [21], Wootters distance [22], Kullback–Shannon (or Tsallis or Rényi) entropy [20], and Jensen–Shannon (or Tsallis or Rényi) divergence [23] are widely adopted to generate the complexity C to characterize the dynamics of complex systems. Moreover, these complexity measures were compared with each other regarding the reliability of properly capturing details of chaotic systems, finding that the choice of the Jensen–Shannon divergence seems more appropriate [24–26]. Furthermore, the complexity measure based on the Jensen–Shannon divergence has been recently introduced as a new tool to differentiate among different chaotic and stochastic systems by representing the complexity and entropy measures in a bi-dimensional space, that is, the so-called entropy-complexity causality plane [27–29]. Alternative to the use of complexity measures, another representation space was introduced by Vignat and Bercher [30], called Shannon–Fisher information plane, which studies the temporal evolution of the Fisher information measure (FIM) as a function of the Shannon entropy. The FIM captures both global and local characteristics of the underlying system, exhibiting some advantages over the aforementioned complexity and entropy measures that are global quantifiers [31].

In this work, we present a comprehensive study of the widely used complexity measures and the FIM, regarding the abilities of these measures to (i) distinguish between chaos and periodicity; (ii) distinguish

among different periodicities; (iii) planar-distinguish among different chaotic regimes; (iv) characterize intrinsic time delay; and (v) planar-distinguish between chaos and noise, in an effort to provide insight into when the measure or plane is more recommendable than the others within the Bandt–Pompe framework. The effect of embedding parameters on the evaluation is also included. The Bandt–Pompe approach to build up probability distribution functions (PDFs) constituted a significant advance in the study of dynamical systems as it incorporates causal information and has no model assumptions [10]. Importantly, studies showed that the Bandt–Pompe PDF is better than the usual histogram or symbolic binary PDF in characterization of chaotic dynamics and planar-behavior representation [25, 26, 32].

The rest of this work is organized as follows: Section 2 introduces the methodology. Section 3 compares the performance of considered measures in characterizing chaotic dynamics. In Sect. 4, simulations are provided to show the reliability of these measures to identify delay dynamics. Likewise, Sect. 5 presents the results for the characterization of chaos and noise. Finally, Sect. 6 concludes.

2 Complexity and information measures within the Bandt–Pompe framework

2.1 The Bandt–Pompe approach

Either the complexity or information measure being utilized, choosing an appropriate probability distribution function (PDF) is crucial. Here, we use the Bandt–Pompe approach [10, 33] to build up the PDF associated with a signal.

Given a time series $\{x_t; t = 1, \dots, n\}$ of length n , an embedding dimension $m > 1$ and delay τ ($m, \tau \in \mathbb{N}$), the ordinal pattern of order m is generated by

$$s \mapsto (x_{s-(m-1)\tau}, x_{s-(m-2)\tau}, \dots, x_{s-\tau}, x_s), \quad (1)$$

which assign to each time s a m -dimensional vector of values pertaining to the times $s, s - \tau, \dots, s - (m - 1)\tau$. The permutation $\pi = (r_0, r_1, \dots, r_{m-1})$ of $(0, 1, \dots, m - 1)$ related to the time s is defined by

$$x_{s-r_{m-1}\tau} \leq x_{s-r_{m-2}\tau} \leq \dots \leq x_{s-r_1\tau} \leq x_{s-r_0\tau}, \quad (2)$$

and $r_i < r_{i-1}$ if $x_{s-r_i\tau} = x_{s-r_{i-1}\tau}$. For all the $m!$ possible permutations π of order m , the probability distribution $P = \{p(\pi_i); i = 1, 2, \dots, m!\}$ is obtained from the time series.

In particular, Bandt and Pompe suggest working with $3 \leq m \leq 7$ for practical purposes. In the present work, we mainly give the results for $4 \leq m \leq 7$ as all simulations work poorly when $m = 3$. Besides, the length n of the time series must satisfy $n \gg m!$ for a reliable statistics [34].

2.2 Statistical complexity measures

For the probability distribution $P = \{p_j, j = 1, 2, \dots, N\}$, the functional form for the statistical complexity measure [23,24,35] is

$$C[P] = Q[P] \cdot H[P], \quad (3)$$

where $H[P]$ is the entropy measure defined as the normalized Shannon entropy,

$$H[P] = S[P]/S_{\max} \quad (4)$$

with $S[P] = -\sum_{j=1}^N p_j \log(p_j)$ and $S_{\max} = S[P_e] = \log(N)$, $P_e = \{1/N, 1/N, \dots, 1/N\}$ is the uniform distribution. $Q[P]$ is defined as the disequilibrium between the two probability distributions P and P_e

$$Q[P] = Q_0 \cdot \mathcal{D}[P, P_e] \quad (5)$$

by adopting some kind of distance $\mathcal{D}[P, P_e]$, and Q_0 is a normalization constant such that $0 \leq Q \leq 1$. Therefore, by definition, the complexity C will vanish either if the system is at equilibrium, implying maximum disorder, or if the system is completely ordered, implying maximal distance from equilibrium [18].

For the choice of distance \mathcal{D} , we consider the following non-trivial statistical measures of distance: Euclidean distance, Wootters distance and Jensen–Shannon divergence, denoted by \mathcal{D}_E , \mathcal{D}_W and \mathcal{D}_{JS} , respectively. For a given H value, there exists a range of possible C values between a minimum C_{\min} and a maximum C_{\max} for each case [24].

2.2.1 Euclidean and Wootters statistical distances

The Euclidean distance in \mathbb{R}^N [21] is given by

$$\mathcal{D}_E[P, P_e] = \|P - P_e\|_E = \sum_{j=1}^N \left\{ p_j - \frac{1}{N} \right\}^2 \quad (6)$$

and accordingly, $Q_0^E = N/(N - 1)$.

The Wootters' statistical distance [22] reads

$$\mathcal{D}_W[P, P_e] = \cos^{-1} \left\{ \sum_{j=1}^N (p_j)^{1/2} \cdot \left(\frac{1}{N} \right)^{1/2} \right\} \quad (7)$$

and $Q_0^W = 1/\cos^{-1} \left\{ \left(\frac{1}{N} \right)^{1/2} \right\}$.

2.2.2 Jensen–Shannon divergence

The distance \mathcal{D}_{JS} is defined in terms of the extensive Jensen–Shannon divergence [23] as follows:

$$\mathcal{D}_{JS}[P, P_e] = S \left[\frac{P + P_e}{2} \right] - \frac{1}{2} S[P] - \frac{1}{2} S[P_e] \quad (8)$$

and $Q_0^{JS} = -2/\left\{ \left(\frac{N+1}{N} \right) \log(N+1) - 2 \log(2N) + \log(N) \right\}$.

2.3 Fisher information measure

A discrete normalized FIM [30,31] is given by

$$F[P] = F_0 \cdot \sum_{j=1}^{N-1} \left\{ (p_{j+1})^{1/2} - (p_j)^{1/2} \right\}^2, \quad (9)$$

where F_0 is a normalization constant and reads

$$F_0 = \begin{cases} 1, & \text{if } p_{j^*} = 1 \text{ for } j^* = 1 \text{ or } j^* = N \\ & \text{and } p_{j^*} = 0 \forall j \neq j^* \\ 1/2, & \text{otherwise.} \end{cases} \quad (10)$$

By definition, the general behavior of the FIM is opposite to that of the Shannon entropy. This is, if a system lies in a very ordered state, we have H tending to 0 and F to 1, and H tends to 1 while F to 0 if the system lies in a very disordered state. Remark that a different ordering of patterns would lead to a different FIM value. Within the Bandt–Pompe framework, we have

$(m!)!$ possibilities. Thus, the specific j -“ordering” of p_j is of great significance. The lexicographic pattern ordering proposed by Lehmer [36,37] is used to assign patterns of indices j .

In the following, complexity measures refer to $C_v[P]$, $v = E, W, JS, F$ and F for the FIM $F[P]$ for clarity.

3 Characterization of chaotic dynamics

In numerical simulations, the first 10^4 or 10^5 iterations are discarded and then n data points are generated for all chaotic systems.

3.1 Discrimination of chaos and periodicity

To evaluate the ability of these complexity and information measures in discriminating among different dynamics, the logistic map is utilized [24,32], i.e.,

$$x_{t+1} = rx_t(1 - x_t) \quad (11)$$

where $0 \leq x_t \leq 1$ and $0 \leq r \leq 4$. When the control parameter $r \geq 3$, the system undergoes a period-doubling bifurcation. For $r > r_\infty \cong 3.5699$, the orbit diagram reveals a mixture of order and chaos.

Figure 1 depicts the bifurcation diagram of logistic map and corresponding LEs for the parameter range $3.5 \leq r \leq 4$. It can be seen that when $r < r_\infty$, the LE remains negative. For $r > r_\infty$, it increases with the parameter r globally and reaches a maximum at $r = 4$, while dropping to negative values or approaching to zero within periodic windows or at period-doubling bifurcation. Correspondingly, the complexity measures C_w and C_{JS} exhibit qualitatively compatible behavior to the LE. They have a very similar appearance over the whole chaotic regime. That is, they take small values for $r < r_\infty$, smoothly grow with the degree of chaoticity and abruptly fall within the periodic windows when $r > r_\infty$. The peaks indicate a local complexity reduction, which coincide with the periodic windows. Importantly, it can be clearly appreciated that C_E , C_w and C_{JS} do distinguish among different periodicities. However, the complexity measure C_E behaves oppositely to C_w and C_{JS} . It assigns higher complexity values to periodic than to chaotic motion and gradually decreases with the parameter r . The complexity measure C_F decreases

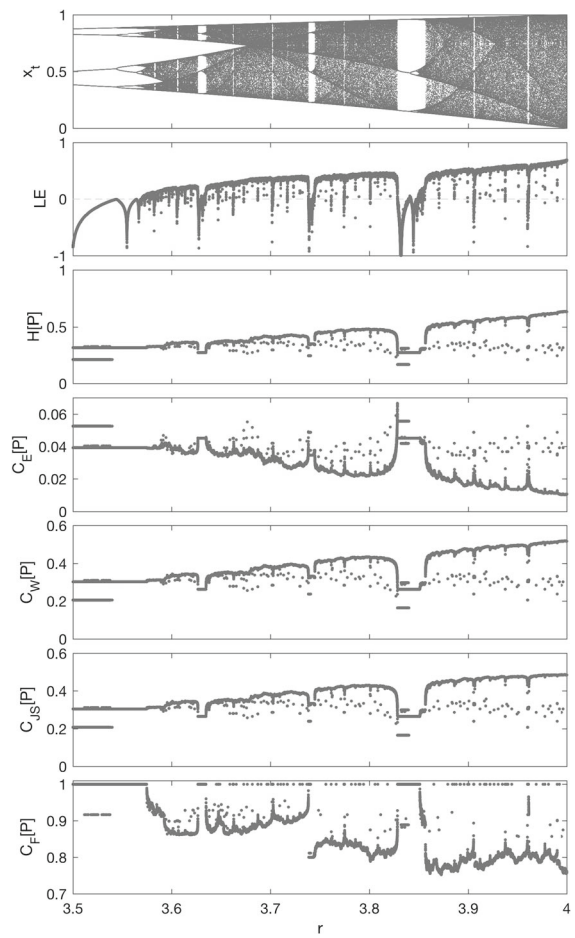


Fig. 1 Logistic map for the parameter range $3.5 \leq r \leq 4$ with step size Δr . Bifurcation diagram ($\Delta r = 0.0002$), LE, H and complexity measures C_v , $v = E, W, JS, F$ ($\Delta r = 1 \times 10^{-5}$) from top to bottom. The PDFs are computed with $m = 6$, $\tau = 1$ and $n = 2^{17}$ using the Bandt–Pompe approach

stepwisely with r , failing to capture essential details of the chaotic dynamics, although all the complexity measures can distinguish periodicity from chaos. However, the C_F does not distinguish among different degrees of periodicity as the others do. The complexity measure C_E characterizes the dynamics of logistic map oppositely to what it is defined.

3.2 Sensitivity to parameters

When generating the Bandt–Pompe PDF, we have three main parameters to decide, i.e., embedding dimension or order m , embedding delay τ and length n . To figure out how these parameters affect the results,

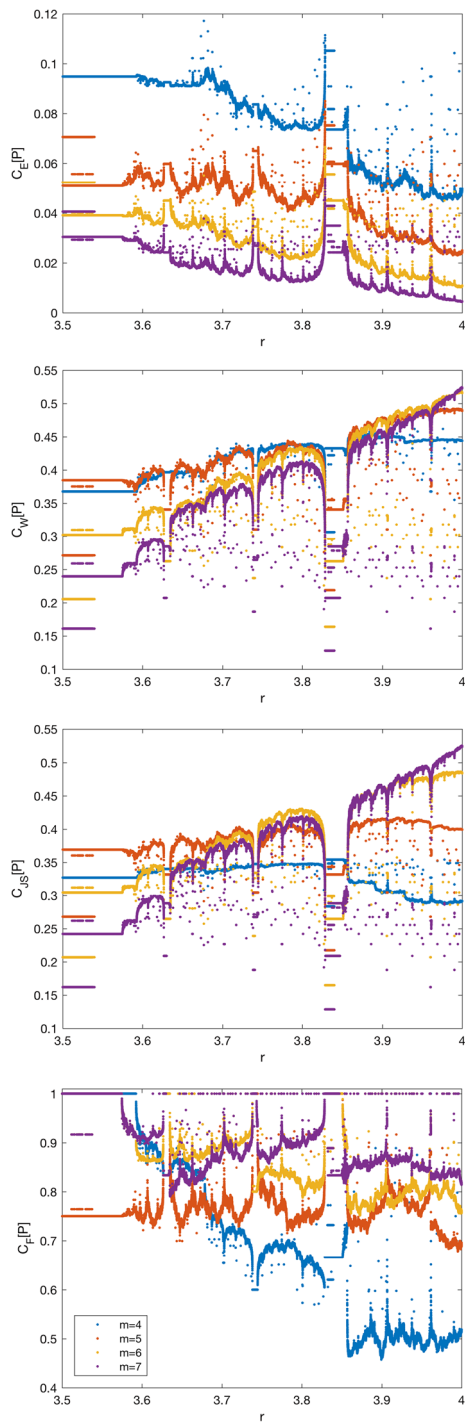


Fig. 2 Complexity measures C_v , $v = E, W, JS, F$, for the logistic map as a function of the control parameter r ($3.5 \leq r \leq 4$ with $\Delta r = 1 \times 10^{-5}$) for $4 \leq m \leq 7$, $\tau = 1$ and $n = 2^{17}$

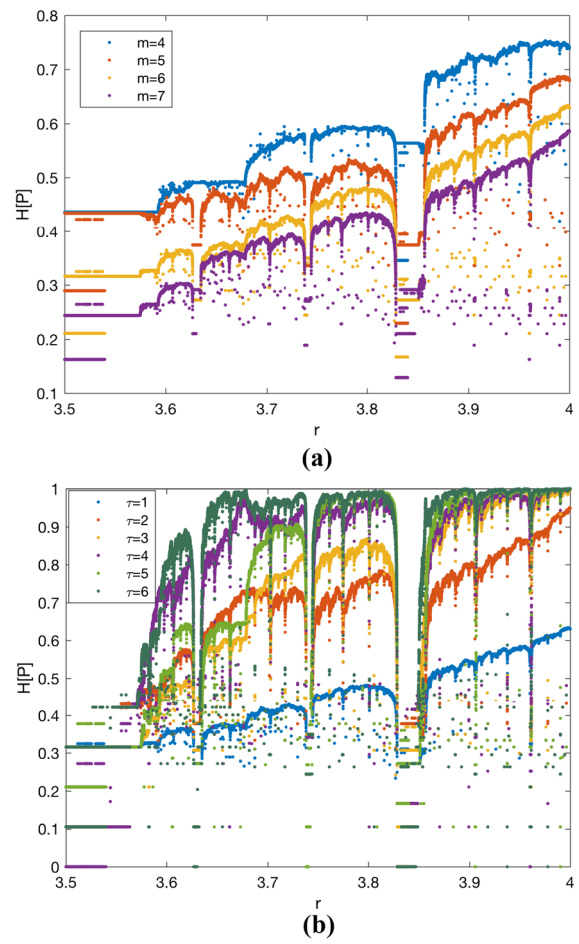


Fig. 3 The normalized Shannon entropy H for the logistic map as a function of the control parameter r ($3.5 \leq r \leq 4$ with $\Delta r = 1 \times 10^{-5}$) for **a** $4 \leq m \leq 7$ and $\tau = 1$, and **b** $m = 6$ and $1 \leq \tau \leq 6$

Fig. 2 presents the complexity measures C_v , $v = E, W, JS, F$ as a function of the control parameter r of logistic map when the embedding dimension m changes from 4 to 7, given $\tau = 1$. For a fixed dimension m , we find that almost the same results can be obtained for varying length $n = 2^k$ with $k = 13, 14, \dots, 17$ for each measure, which demonstrates that length n barely affects the evaluation as long as it satisfies $n \gg m!$. Thus, only the results for $n = 2^{17}$ are provided. As a reference, we also show the results for the entropy H in Fig. 3a. It can be seen that the embedding dimension does not alter the appearances of H and C_E . However, when $r > 3.9$, C_W decreases for $m = 4$ and C_{JS} decreases for $m = 5$. Moreover, C_{JS} presents a decreasing trend for $r > 3.85$ and $m = 4$. It has a sim-

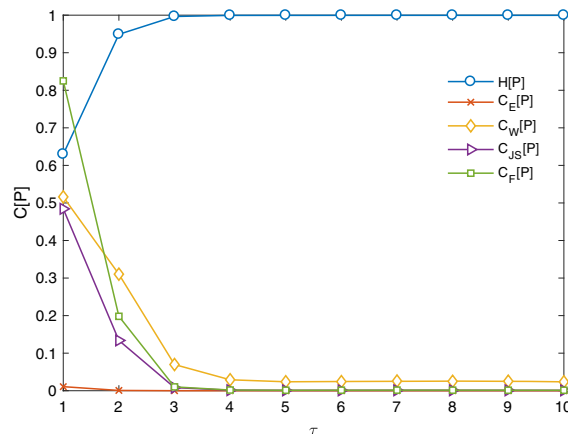


Fig. 4 Complexity measures C_v , $v = E, W, JS, F$ and entropy H for the logistic map ($r = 4$) as a function of the embedding delay τ for $m = 6$ and $n = 2^{17}$. Same results can be obtained for τ up to 400

ilar appearance to the LE for $m = 6, 7$, more sensitive to the embedding dimension than C_W . C_F works well only for $m = 6$. Clearly, the C_F values corresponding to periodic motions largely drop rather than increase for $3.6 < r < 3.8$ and $m = 4$. Besides, when $m = 5$, C_F is almost stable over the whole range, and it shows smaller values in the less chaotic region $3.6 < r < 3.7$ for $m = 7$. For different m , the global trends of C_F are different, implying its high sensitivity to the embedding dimension.

Furthermore, to study the effect of embedding delay τ on the evaluation, we show the complexity measures C_v , $v = E, W, JS, F$ and entropy H for the fully chaotic logistic map ($r = 4$) as a function of τ in Fig. 4. Obviously, the entropy H approaches to its maximum value of $H_{\max} = 1$ that corresponds to complete randomness when $\tau \geq 3$. Accordingly, all complexity measures tend to zero, indicating that large delay τ invalidates all measures. Moreover, Fig. 5 displays these complexity measures as a function of the control parameter r for different delays $1 \leq \tau \leq 6$, given $m = 6$. It is clear that all measures are severely affected by the varying embedding delay. Specifically, C_W and C_{JS} are only valid at $\tau = 1$ as they globally decrease with the increasing r and assign higher values to some periodic windows for $\tau \geq 2$. C_E and C_F are not proper for $\tau \geq 3$ because they assign nearly zero values to the regions of chaos, e.g., chaotic regions in [3.85, 4]. The results for the entropy H are shown in Fig. 3b. As expected, H tends to the highest value of $H_{\max} = 1$ in some chaotic regions when $\tau \geq 3$.

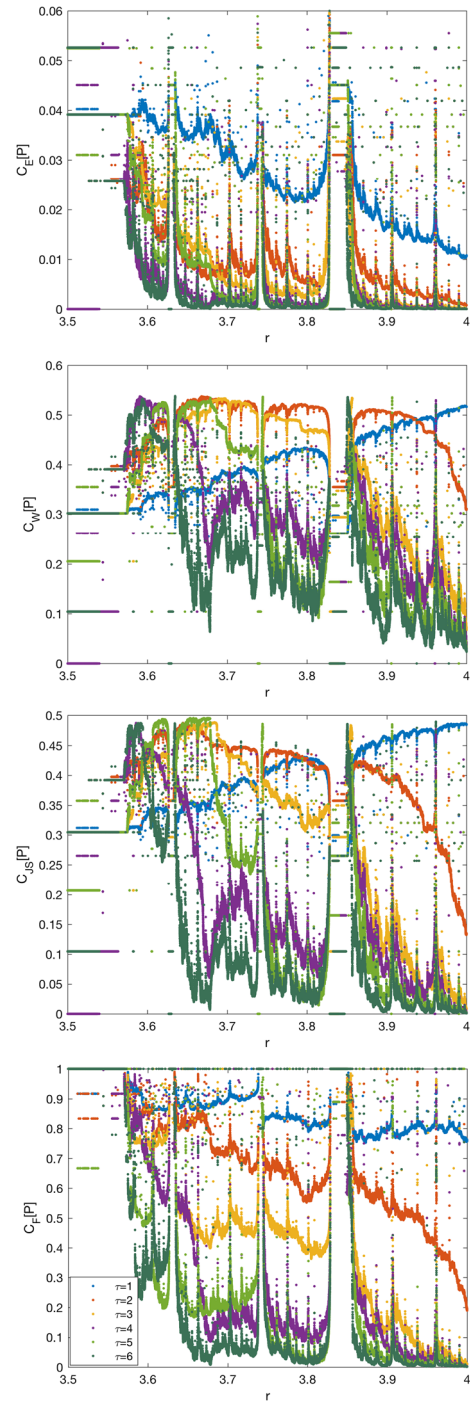


Fig. 5 Complexity measures C_v , $v = E, W, JS, F$, for the logistic map as a function of the control parameter r ($3.5 \leq r \leq 4$) with $\Delta r = 1 \times 10^{-5}$ for $1 \leq \tau \leq 6$, $m = 6$ and $n = 2^{17}$

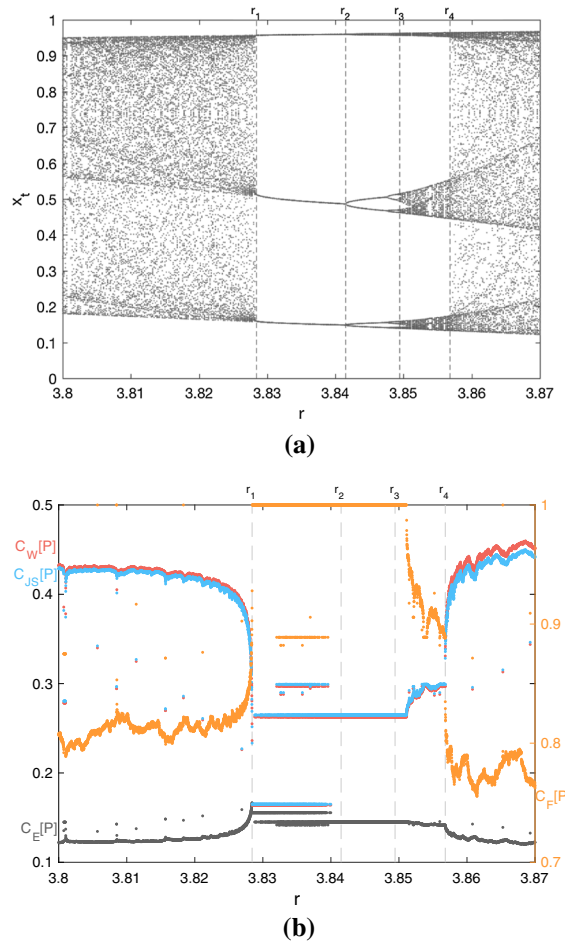


Fig. 6 **a** Bifurcation diagram ($\Delta r = 0.0002$) and **b** complexity measures C_v , $v = E, W, JS, F$ ($\Delta r = 1 \times 10^{-5}$) for logistic map within the parameter range $3.8 \leq r \leq 3.87$ with Δr for $m = 6$, $\tau = 1$ and $n = 2^{17}$. The results for C_E are translated vertically by C_E plus 0.1. The vertical dashed lines represent different dynamical windows described in the text

3.3 Planar characterization of chaotic regimes

As mentioned above, when r grows beyond r_∞ , the dynamics of logistic map include a mixture of order and chaos. Particularly, we consider the parameter range $3.8 \leq r \leq 3.87$, where the logistic map goes through chaos-period transitions at $r_1 \cong 3.82842$, $r_2 \cong 3.8415$, $r_3 \cong 3.84943$ and $r_4 \cong 3.85681$ [37]. The dynamics within this parameter range can be briefly separated to five regions: chaos 1 for $3.8 \leq r < r_1$, period-3 for $r_1 < r < r_2$, period-doubling for $r_2 < r < r_3$, chaos 2 with periodic window for $r_3 < r < r_4$, and chaos 3 for $r_4 < r \leq 3.87$. An enlarged bifurcation diagram of

logistic map within this parameter range is displayed in Fig. 6a. Figure 6b shows the corresponding complexity measures, whose values display a trend that clearly distinguishes among different chaotic behaviors (chaos 1, 2 and 3 zones), respectively. Based on previous analyses, the PDFs are computed with $m = 6$, $\tau = 1$ and $n = 2^{17}$.

The planar representation of the five dynamic regimes is shown in Fig. 7. Clearly, the $H \times C_E$ and $H \times C_F$ planes produce the better distinction (planar localization without overlapping) between different regimes associated with the values of r . In the two planes, the characteristics for different dynamic regimes are more clearly evidenced. Each regime is located at different planar locations. By comparison, the three chaotic zones distribute nearly alone a line in the $H \times C_W$ and $H \times C_{JS}$ planes, and it is difficult to differ one from the others.

Overall, regarding the performance of the complexity measures in characterizing chaotic dynamics, we can conclude that (i) the four complexity measures C_v , $v = E, W, JS, F$ can distinguish periodicity from chaos; (ii) C_W and C_{JS} exhibit qualitatively similar characterization behavior, behaving in a compatible manner with the LE; (iii) C_F cannot capture subtle changes of the chaotic dynamics or distinguish among different degrees of periodicity; (iv) C_E and C_F better distinguish among different chaotic regions via the entropy-complexity plane; (v) C_E can capture the change of degrees of periodicity but violates its definition; (vi) the embedding dimension m has an important effect on all complexity measures except C_E , and higher value of m , e.g., $m = 6$ or 7, is more appropriate when characterizing the chaotic dynamics. Moreover, the embedding delay τ affects the validity of all the measures and they are compatible to the LE when there is no delay, i.e., $\tau = 1$, or with small delay $\tau = 2$. All considered measures are not affected by the choice of length n if it meets the condition.

4 Identification of delay dynamics

In a traditional way, the Bandt–Pompe approach works with no embedding delay, i.e., $\tau = 1$. However, there are studies showing that H and C_{JS} would change with embedding delay τ for nonlinear dynamical chaotic systems, but be constant for self-similar stochastic processes [38–40]. Moreover, they are able to identify the

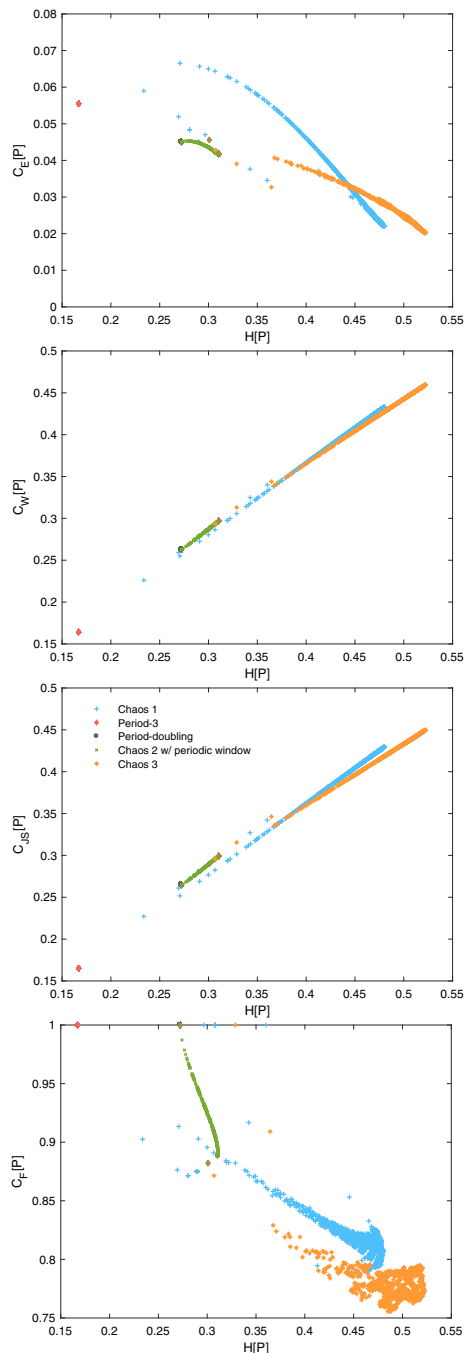


Fig. 7 Entropy-complexity planes $H \times C_v$, $v = E, W, JS, F$, for the logistic map within the parameter range $3.8 \leq r \leq 3.87$ with $\Delta r = 1 \times 10^{-5}$. The parameter does not explicitly appear in the graph

characteristic time delay of a delayed chaotic system as H is minimized and C_{JS} is maximized when the embedding delay matches the intrinsic time delay of

the system [39]. Therefore, other values of the embedding delay could provide additional information, and a proper selection of it is of great significance to reveal the intrinsic dynamics of the underlying system. In order to evaluate how the embedding delay is related to the intrinsic time delay for the considered complexity measures, we analyze their delay-dependent behavior.

The time-delayed system of interest is the classic Mackey–Glass equation [41], which is given by

$$\frac{dx}{dt} = -x + \frac{ax(t - \tau_s)}{1 + x^c(t - \tau_s)} \quad (12)$$

with $a = 2$, $c = 10$, and $\tau_s = 60$, where the system operates in a high-dimensional chaotic regime. The Mackey–Glass time series is generated by the fourth-order Runge–Kutta method with an integration step $\Delta t = 0.2$ [42]. Figure 8 plots the complexity measures C_v , $v = E, W, JS, F$, as a function of the embedding delay τ for different dimensions $4 \leq m \leq 7$. It is obvious that all the measures have a most pronounced maximum when the embedding delay τ approximates τ_s of the system, i.e., $\tau \sim 300$ ($\tau_s/\Delta t = 300$), specifically, $\tau = 302$ for all, with other maxima related to (sub-) harmonics of the characteristic time delay τ_s of the system. Moreover, the scale identification is independent of the embedding dimension m , except that C_w has an increase in the baseline for $m = 7$.

It was mentioned that H and C_{JS} present no clear minima or maxima for the non-delayed Lorenz system [39]. Likewise, for a comprehensive evaluation, we consider the three-dimensional Lorenz system, which is

$$\begin{cases} \dot{x} = s(x - y) \\ \dot{y} = x(r - z) - y \\ \dot{z} = xy - bz \end{cases} \quad (13)$$

with $s = 10$, $b = 8/3$, and $r = 28$ in a chaotic region [43]. The Lorenz series is obtained by the Euler's method with an integration step $\Delta t = 0.01$ [44]. Accordingly, Fig. 9 gives the complexity measures C_v , $v = E, W, JS, F$ and entropy H for the x -coordinate series as a function of the embedding delay τ , given $m = 6$. As expected, the entropy H grows with increasing τ and rapidly approaches its maximum value as $\tau \rightarrow \infty$ [38]. Besides, it is clear that all complexity measures increase and then decrease at relatively small delay, say $\tau < 30$. At large scales, all complex-

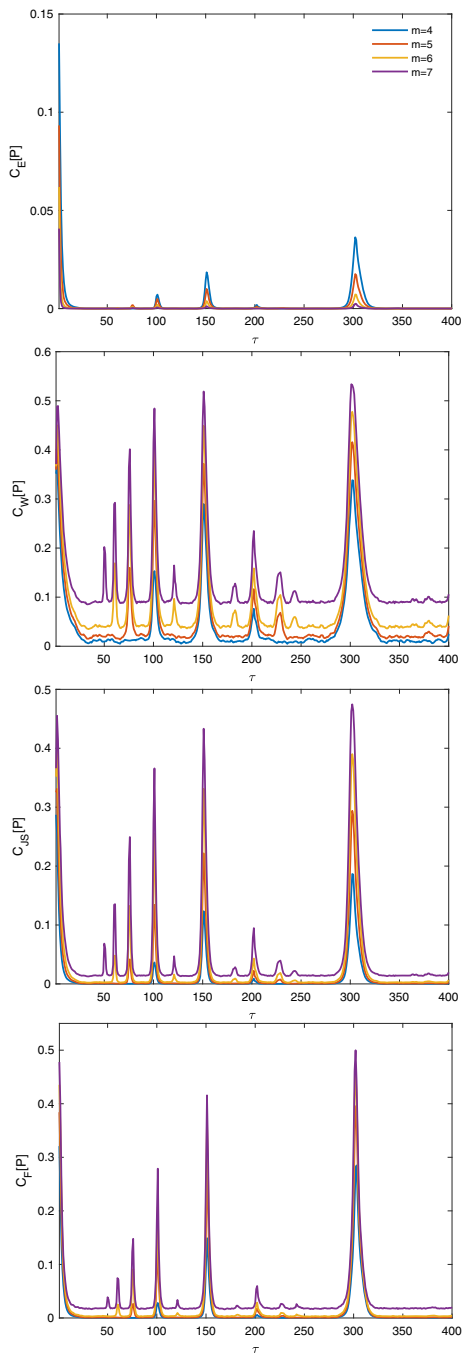


Fig. 8 Complexity measures C_v , $v = E, W, JS, F$, for the Mackey–Glass system as a function of the embedding delay τ for $4 \leq m \leq 7$ and $n = 2^{17}$ with an integration step $\Delta t = 0.2$

ity measures decrease to zero with the increase in τ and show no pronounced maxima that could lead to spurious delay identification. Thus, the nonlinear dynamical behavior of the system appears to be random rather than

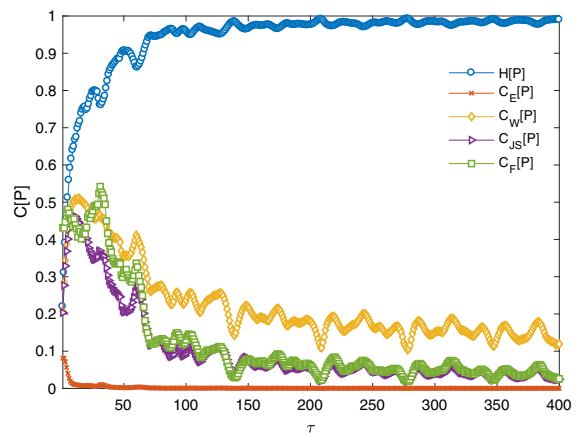


Fig. 9 Complexity measures C_v , $v = E, W, JS, F$ and entropy H for the Lorenz system (x -coordinate) as a function of the embedding delay τ for $m = 6$ and $n = 2^{17}$

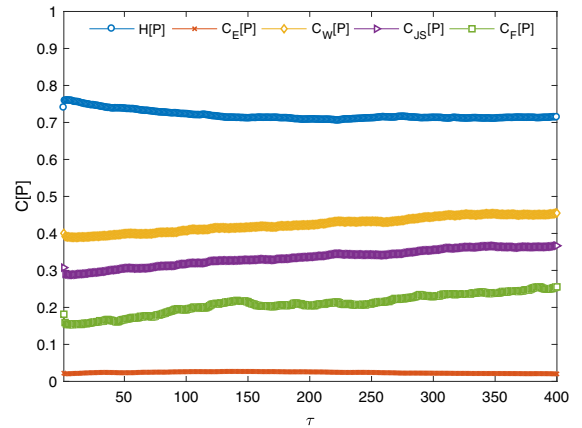


Fig. 10 Complexity measures C_v , $v = E, W, JS, F$ and entropy H for the f^{-k} noise ($k = 2.5$) as a function of the embedding delay τ for $m = 6$ and $n = 2^{17}$

chaotic for large values of τ , implying that the intrinsic nonlinear deterministic dynamics of the system are more properly revealed by low or intermediate embedding delays. Similar results can be obtained for the y - and z -coordinates of the Lorenz system, respectively.

Other than considering the above nonlinear deterministic chaotic systems, as a comparison, we plot the delay-dependent complexity measures for the f^{-k} ($k = 2.5$) stochastic noise [27, 45], which is scale-free, as a function of the embedding delay τ in Fig. 10. Similar to what has found for H and C_{JS} in [40], no extrema are detected by C_E , C_W or C_F , and they are nearly constant over the whole range of τ .

In short, the four kinds of complexity measures have no distinctive difference in identifying the delay dynamics of deterministic chaotic systems and self-similar stochastic systems. They can detect the intrinsic delay of delayed chaotic systems precisely and display no clear extrema for non-delayed chaotic systems at large scales and self-similar stochastic systems at all scales. Consequently, the three types of systems show different patterns in the two-dimensional entropy-complexity planes and are easy to be discriminated from each other, as illustrated in Fig. 11.

5 Discrimination between chaos and noise

5.1 Description of chaotic and stochastic systems

To evaluate the performance of complexity measures in planar-discriminating chaos from noise, we consider several chaotic and stochastic systems here, namely (a) chaotic maps [28, 46, 47], including (i) non-invertible maps: logistic map ($r = 4$), sine map, cubic map, Schuster map ($1.5 \leq z \leq 2.5$); (ii) dissipative maps: Hénon map, Tinkerbell map, Burgers' map; (iii) conservative maps: Arnold's cat map, Gingerbreadman map, Lorenz map (x -minimal values of the three-dimensional Lorenz system); and (b) stochastic processes [27, 45, 48], including (i) f^{-k} noise ($0 \leq k \leq 3$) and (ii) fractional Brownian motion (fBm, $1.2 \leq \alpha \leq 2.8$) and fractional Gaussian noise (fGn, $-0.8 \leq \alpha \leq 0.8$).

Note that high-dimensional chaotic dynamical systems exhibit forbidden patterns and there is a minimum dimension m_{\min} such that forbidden patterns cannot appear for $m < m_{\min}$ [47]. Additionally, on the basis of previous results, the embedding dimension $m = 6$, embedding delay $\tau = 1$ and length $n = 2^{17}$ are adopted to generate the Bandt-Pompe PDFs. For the Hénon map and Arnold's cat map, both the x - and y -coordinates have the same ordinal structure and they locate at the same point in the entropy-complexity planes. Therefore, only the results from respective x -coordinates are presented. The y -coordinate of Gingerbreadman map remains the same and thus not considered as well.

5.2 Planar separation of chaos and noise

Figure 12 shows the entropy-complexity planes for considered chaotic and stochastic systems. For the

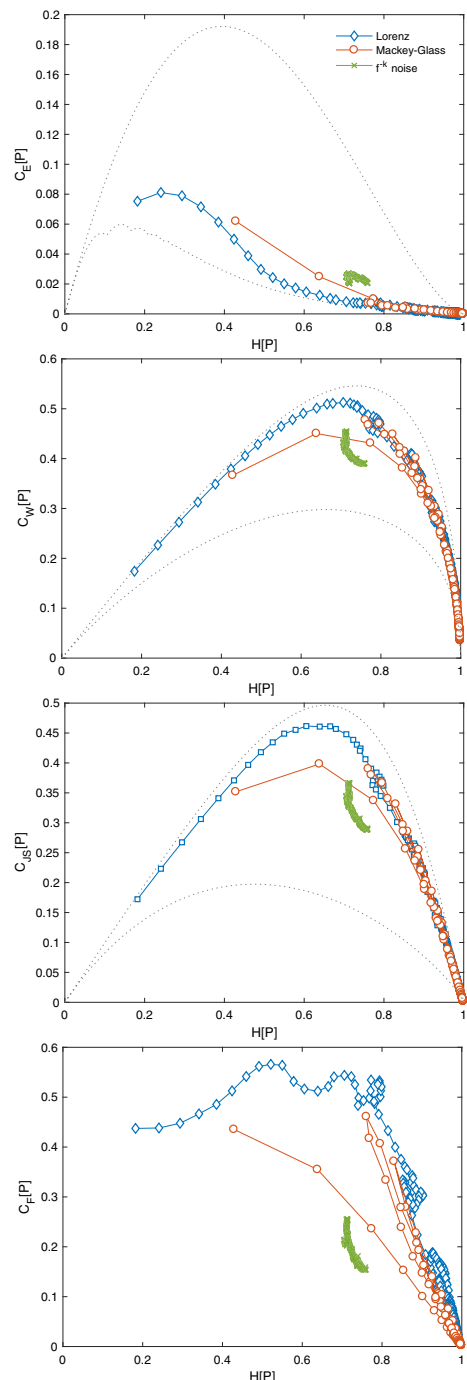


Fig. 11 Entropy-complexity planes $H \times C_v$, $v = E, W, JS, F$, for the Lorenz, Mackey-Glass chaotic system and stochastic f^{-k} noise as a function of the embedding delay τ for $m = 6$ and $n = 2^{17}$. The parameter does not explicitly appear in the graph

stochastic processes, in general, they have entropy $H > 0.45$ and low complexity values $C < 0.4$ ($C_E <$

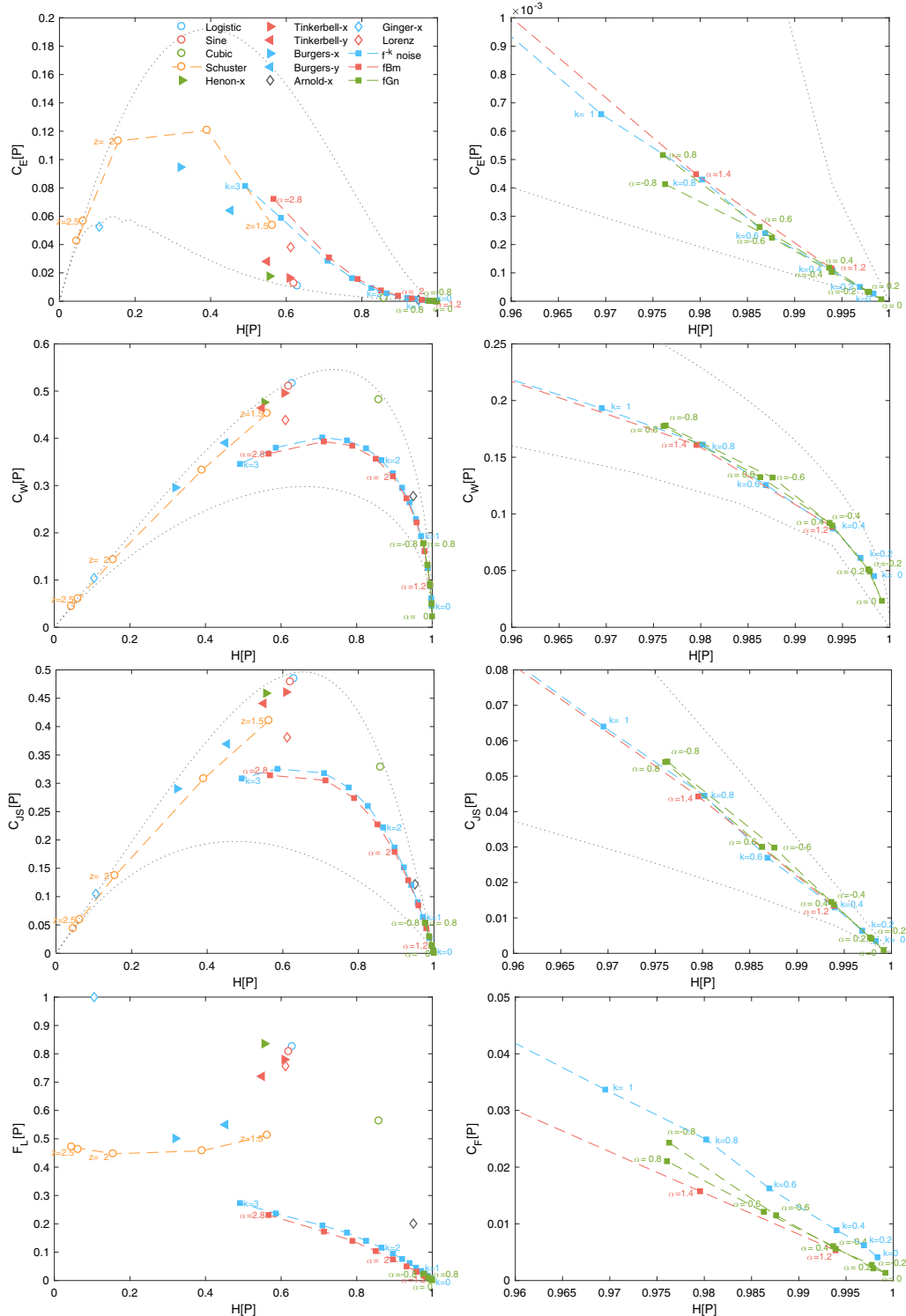


Fig. 12 (left column) Entropy-complexity planes $H \times C_v$, $v = E, W, JS, F$, for different chaotic and stochastic systems. (right column) Enlargement of corresponding planes near the point $(1, 0)$

0.1), almost equidistant to the curves of $C_{\min}[H]$ and $C_{\max}[H]$ (if any) in respective planes. In addition, the f^{-k} noise and fBm exhibit close complexity and entropy values. Their entropy values both decrease as the correlation grows. Persistent fBm is more complex than anti-persistent fBm. For the fGn, persistent and anti-persistent ones display approximately symmetric complexity values, which locate near the lower-right corner of respective planes (see the enlarged plots in the right column of Fig. 12). When $\alpha = 0$, the fGn becomes white noise exhibiting the highest entropy $H \cong 1$ and lowest complexity values $C \cong 0$. When $k = 0$, the correlation of f^{-k} noise vanishes as well. Chaotic maps are mostly located at the medium-entropy region with $0.3 < H < 0.65$. The Arnold's cat map has a high entropy value of $H = 0.9496$, due to its homogeneous structure. On the contrary, the Gingerbreadman map displays low entropy $H = 0.1054$ for its embedded periodic structure in phase space [49]. Schuster maps exhibit laminar regions separated by chaotic bursts [27]. When the parameter z decreases, the size of laminar regions diminishes and the system becomes more similar to a fully chaotic one. As a result, its entropy value increases from 0.0267 to 0.5618 as the parameter z decreases from 2.5 to 1.5, being close to those of chaotic maps. Therefore, in the four planes, chaotic maps are mainly at the left half plane, while stochastic processes are at the right half one, indicating the intrinsic difference of chaos to noise.

Moreover, it can be seen that all the four planes work well for stochastic noises, but different for the case of chaotic maps. In the $H \times C_{JS}$ plane, the locations of chaotic maps always remain near to the maximum complexity curve, which is consistent with [27]. For non-invertible and dissipative chaotic maps, they show generally higher values of complexity than stochastic processes. Moreover, a similar observation also holds for the $H \times C_w$ plane. Complexity measures C_w and C_{JS} represent considered chaotic and stochastic systems in respective entropy-complexity plane in a qualitatively similar manner, as expected. Both complexity measures can characterize different degrees of correlation of stochastic processes and distinguish chaotic systems from stochastic noises. Besides, locations of chaotic maps are slightly closer to the maximum complexity curve in the $H \times C_w$ plane than in the $H \times C_{JS}$ plane. The complexity measure C_E behaves oppositely regarding the characterization behavior of chaos and periodicity, as illustrated in Fig. 1. As a consequence,

chaotic maps are mainly found in close vicinity to its minimum complexity curve in the $H \times C_E$ plane, displaying much lower complexity values than stochastic processes. Moreover, the $H \times C_E$ plane poorly characterizes the planar behavior of Burger's map and Schuster map, whose locations are far from the minimum complexity curve and much close to stochastic processes. Unlike C_E , C_F assigns higher values to periodic systems by definition, the $H \times C_F$ plane can nevertheless separate chaos from noise properly. It is clear to see that in the $H \times C_F$ plane, chaotic maps are mainly located in the upper plane with $C_F > 0.4$, while stochastic processes present lower complexity values of $C_F < 0.3$.

Similar results are obtained when the analysis is performed for other m -values ($m = 5, 7$). Moreover, the planar separation of chaos and noise becomes more clear when they are represented in higher-dimensional planes ($m = 7$) except for the $H \times C_E$ plane. Chaos and noise cannot be properly distinguished with dimension $m < 5$ for any plane.

5.3 Effect of extrinsic noise

In order to test the effect of extrinsic noise on the results, Gaussian white noise is added to the original noise-free logistic map and different noise levels (NL) are considered. The NL is defined by the standard deviation of the noise divided by the standard deviation of the original signal. Associated entropy-complexity planes are depicted in Fig. 13, where the values related to the pure white noise and f^{-k} stochastic process are also displayed to illustrate the reliability of these planes in separating noisy chaos from noise. Considering the poor performance of C_E and similar characterization behavior of C_w and C_{JS} , only the entropy-complexity planes $H \times C_{JS}$ and $H \times C_F$ are compared here.

From Fig. 13, it is easy to see that in both planes, the main effect of additive noise is to shift the original logistic map localization toward the region of pure noise. When the NL increases, the value of entropy increases and value of complexity decreases, without overlapping the planar localization of pure noise. Moreover, a clear differentiation can be appreciated between the noisy logistic map and the stochastic f^{-k} processes in the $H \times C_F$ plane. By comparison, in the $H \times C_{JS}$ plane, the planar location of the noisy logistic map tends close to and finally coincides with those of f^{-k}

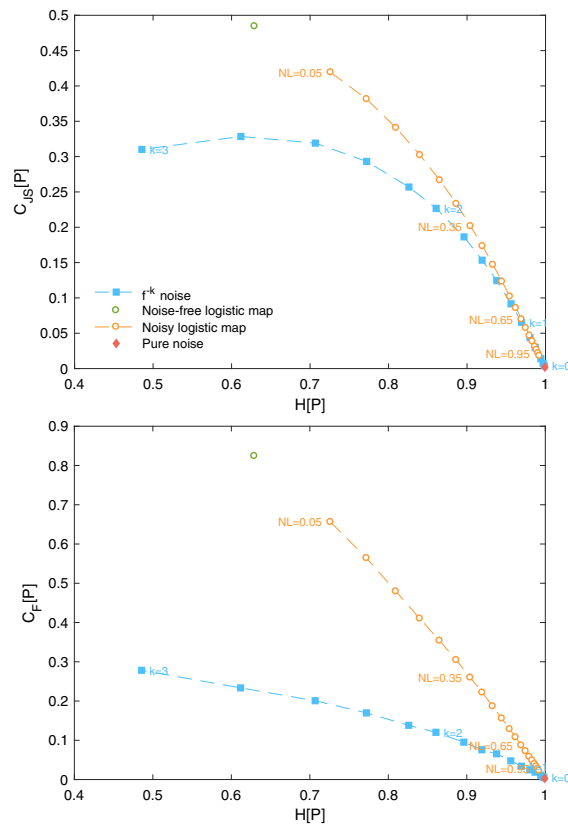


Fig. 13 Entropy-complexity planes $H \times C_{JS}$ and $H \times C_F$ for the logistic map polluted by additive noise with different NLs ($NL = 0.05, 0.1, \dots, 0.95, 1$ with $\Delta NL = 0.05$). Results for the pure white noise and f^{-k} stochastic noise are also displayed

stochastic noise as the NL gets larger. Therefore, the entropy-complexity plane $H \times C_F$ is more robust than the $H \times C_{JS}$ plane in distinguishing chaos from noise when the chaotic system is polluted with noise. The $H \times C_{JS}$ plane is reliable when the level of additive noise is not very high, and it is reasonable to infer that it applies to the $H \times C_W$ plane as well.

In general, regarding the performance of entropy-complexity planes in discriminating between chaos and noise, conclusions can be drawn that, (i) stochastic noises have generally higher entropy values than chaotic maps; (ii) all the four entropy-complexity planes can characterize different degrees of correlation of stochastic processes; (iii) the $H \times C_v$, $v = W, JS, F$ planes can properly distinguish chaotic systems from stochastic noises; (iv) the locations of chaotic maps are near to the theoretical maximum complexity curve in the $H \times C_W$ and $H \times C_{JS}$ planes, while stochas-

tic processes are nearly equidistant to the theoretical maximum and minimum complexity curves; (v) in the $H \times C_F$ plane, chaotic maps mainly locate at the upper half plane, while stochastic processes are at the lower half plane; (vi) the $H \times C_F$ plane is robust to extrinsic noise, while $H \times C_W$ and $H \times C_{JS}$ are sensitive to noise with high NL; and (vii) the $H \times C_E$ plane works better for stochastic processes and it cannot characterize chaos properly.

6 Discussion and conclusion

In this work, we have evaluated the feasibility of four kinds of complexity or information measures to appropriately characterize chaos and noise within the Bandt–Pompe framework. The results are summarized in Table 1. Generally, the complexity measures based on the Wootters distance C_W and Jensen divergence C_{JS} can appropriately detect subtle changes of chaotic dynamics, but fail to differentiate among different chaotic zones through the entropy-complexity plane. Besides, the complexity measures C_W and C_{JS} exhibit compatible characterization behavior. In theory, physicists believe that C_{JS} is better than C_W and C_E because it is an intensive quantity [24]. In practice, the C_W performs slightly better than C_{JS} in characterizing chaos and noises via the entropy-complexity plane, and it is also less sensitive to the embedding parameters. The FIM is an information measure but performs compatible to these complexity measures. To planar-distinguish different chaotic regimes or planar-separate chaos and noise, the entropy-information plane based on the FIM is an optimal choice. It is also more insensitive to additive noises. For the identification of delay dynamics of chaotic and stochastic systems, the four kinds of measures are compatible to each other. However, by definition, the complexity measure based on the Euclidean distance C_E is invalid using the Bandt–Pompe probabilities, as it assigns higher complexity value to periodic than chaotic unity.

In summary, the selection of an appropriate distance or information measure or the selection of probability space is critical to practical purposes. So are the embedding parameters. Though the Bandt–Pompe approach to generate PDFs is superior at some cases, it is not universal. Within the Bandt–Pompe framework and with properly selected parameters, the complexity measures C_W and C_{JS} are more applicable to capture dynamic

Table 1 Summary of the performance of complexity measures C_v , $v = E, W, JS, F$ using the Bandt–Pompe PDF. Checkmark for yes, cross for no and bar for not considered

	C_E	C_W	C_{JS}	C_F
Characterize chaotic dynamics				
Capture subtle details	✓	✓	✓	✗
Distinguish chaos from periodicity	✓	✓	✓	✓
Distinguish among degrees of periodicity	✓	✓	✓	✗
Planar-separate chaotic zones	✓	✗	✗	✓
Identify delay dynamics	✓	✓	✓	✓
Planar-discriminate between chaos and noise				
Characterize chaos	✗	✓	✓	✓
Characterize noise	✓	✓	✓	✓
Separate chaos and noise	✗	✓	✓	✓
Robust to additive noises	-	low NL	low NL	✓
Insensitivity to parameters				
Length n	✓	✓	✓	✓
Embedding dimension m	$C_E > C_W > C_{JS} > C_F$			
Embedding delay τ	$C_E = C_F > C_W = C_{JS}$			
Consistent with the original definition	✗	✓	✓	✓

changes of chaos, and the information measure FIM is more suitable for characterizing chaos and noise in the two-dimensional plane. The complexity measure C_E is not recommended at any cases.

Acknowledgements We acknowledge the financial supports from the National Natural Science Foundation of China (61771035, 61673005) and the Fundamental Research Funds for the Central Universities (2019YJS203, 2018JBZ104, 2019RC049).

Compliance with Ethical Standards

Conflict of interest The authors declare that they have no conflict of interest.

References

- Shannon, C.E.: A mathematical theory of communication. *Bell Syst. Tech. J.* **27**(3), 379–423 (1948)
- Cover, T.M., Thomas, J.A.: Elements of Information Theory. Wiley, Hoboken (2012)
- Mandelbrot, B.B.: Self-affine fractals and fractal dimension. *Phys. Scr.* **32**(4), 257 (1985)
- Theiler, J.: Estimating fractal dimension. *JOSA A* **7**(6), 1055–1073 (1990)
- Wolf, A., Swift, J.B., Swinney, H.L., Vastano, J.A.: Determining Lyapunov exponents from a time series. *Physica D* **16**(3), 285–317 (1985)
- Eckmann, J.P., Ruelle, D.: Ergodic theory of chaos and strange attractors. In: The Theory of Chaotic Attractors (pp. 273–312). Springer, New York (1985)
- Cornfeld, I.P., Fomin, S.V., Sinai, Y.G.: Ergodic Theory, vol. 245. Springer, Berlin (2012)
- Adler, R.L., Konheim, A.G., McAndrew, M.H.: Topological entropy. *Trans. Am. Math. Soc.* **114**(2), 309–319 (1965)
- Latora, V., Baranger, M.: Kolmogorov-Sinai entropy rate versus physical entropy. *Phys. Rev. Lett.* **82**(3), 520 (1999)
- Bandt, C., Pompe, B.: Permutation entropy: a natural complexity measure for time series. *Phys. Rev. Lett.* **88**(17), 174,102 (2002)
- Bernaola-Galván, P., Oliver, J.L., Román-Roldán, R.: Decomposition of DNA sequence complexity. *Phys. Rev. Lett.* **83**(16), 3336 (1999)
- Goldberger, A.L., Peng, C.K.: Genomic classification using an information-based similarity index: application to the SARS coronavirus. *J. Comput. Biol.* **12**(8), 1103–1116 (2005)
- Kantz, H., Kurths, J., Mayer-Kress, G.: Nonlinear Analysis of Physiological Data. Springer, Berlin (2012)
- Yang, A.C.C., Peng, C.K., Yien, H.W., Goldberger, A.L.: Information categorization approach to literary authorship disputes. *Phys. A* **329**(3–4), 473–483 (2003)
- Bialek, W., Nemenman, I., Tishby, N.: Predictability, complexity, and learning. *Neural Comput.* **13**(11), 2409–2463 (2001)
- Crutchfield, J.P., Feldman, D.P.: Synchronizing to the environment: information-theoretic constraints on agent learning. *Adv. Complex Syst.* **4**(02n03), 251–264 (2001)

17. Nemenman, I.: Information theory and learning: a physical approach. preprint physics (2000). [arXiv:physics/0009032v1](https://arxiv.org/abs/physics/0009032v1)
18. Shiner, J.S., Davison, M., Landsberg, P.T.: Simple measure for complexity. Phys. Rev. E **59**(2), 1459 (1999)
19. Grassberger, P.: Toward a quantitative theory of self-generated complexity. Int. J. Theor. Phys. **25**(9), 907–938 (1986)
20. Aczél, J., Daróczy, Z.: On measures of information and their characterizations. New York, p. 168 (1975)
21. Lopez-Ruiz, R., Mancini, H.L., Calbet, X.: A statistical measure of complexity. Phys. Lett. A **209**(5–6), 321–326 (1995)
22. Wootters, W.K.: Statistical distance and Hilbert space. Phys. Rev. D **23**(2), 357 (1981)
23. Lamberti, P., Martin, M., Plastino, A., Rosso, O.: Intensive entropic non-triviality measure. Phys. A **334**(1–2), 119–131 (2004)
24. Martin, M., Plastino, A., Rosso, O.: Generalized statistical complexity measures: geometrical and analytical properties. Phys. A **369**(2), 439–462 (2006)
25. Kowalski, A.M., Martin, M.T., Plastino, A., Rosso, O.A., Casas, M.: Distances in probability space and the statistical complexity setup. Entropy **13**(6), 1055–1075 (2011)
26. Rosso, O.A., Martín, M., Larrondo, H.A., Kowalski, A., Plastino, A.: Generalized statistical complexity: a new tool for dynamical systems. In: Concepts and Recent Advances in Generalized Information Measures and Statistics, pp. 169–215 (2013)
27. Rosso, O., Larrondo, H., Martín, M., Plastino, A., Fuentes, M.: Distinguishing noise from chaos. Phys. Rev. Lett. **99**(15), 154,102 (2007)
28. Ribeiro, H.V., Jauregui, M., Zunino, L., Lenzi, E.K.: Characterizing time series via complexity-entropy curves. Phys. Rev. E **95**(6), 062,106 (2017)
29. Jauregui, M., Zunino, L., Lenzi, E.K., Mendes, R.S., Ribeiro, H.V.: Characterization of time series via rényi complexity-entropy curves. Phys. A **498**, 74–85 (2018)
30. Vignat, C., Bercher, J.F.: Analysis of signals in the fisher-shannon information plane. Phys. Lett. A **312**(1–2), 27–33 (2003)
31. Olivares, F., Plastino, A., Rosso, O.A.: Contrasting chaos with noise via local versus global information quantifiers. Phys. Lett. A **376**(19), 1577–1583 (2012)
32. Rosso, O.A., De Micco, L., Plastino, A., Larrondo, H.A.: Info-quantifiers' map-characterization revisited. Physica A **389**(21), 4604–4612 (2010)
33. Packard, N.H., Crutchfield, J.P., Farmer, J.D., Shaw, R.S.: Geometry from a time series. Phys. Rev. Lett. **45**(9), 712 (1980)
34. Staniak, M., Lehnertz, K.: Parameter selection for permutation entropy measurements. Int. J. Bifurc. Chaos **17**(10), 3729–3733 (2007)
35. Martin, M., Plastino, A., Rosso, O.: Statistical complexity and disequilibrium. Phys. Lett. A **311**(2–3), 126–132 (2003)
36. <http://www.keithschwarz.com/interesting/code/factoradic-permutation/FactoradicPermutation.hh.html>
37. Olivares, F., Plastino, A., Rosso, O.A.: Ambiguities in bandt-pompe's methodology for local entropic quantifiers. Physica A **391**(8), 2518–2526 (2012)
38. Bandt, C.: Ordinal time series analysis. Ecol. Model. **182**(3–4), 229–238 (2005)
39. Zunino, L., Soriano, M.C., Fischer, I., Rosso, O.A., Mirasso, C.R.: Permutation-information-theory approach to unveil delay dynamics from time-series analysis. Phys. Rev. E **82**(4), 046212 (2010)
40. Zunino, L., Soriano, M.C., Rosso, O.A.: Distinguishing chaotic and stochastic dynamics from time series by using a multiscale symbolic approach. Phys. Rev. E **86**, 046210 (2012)
41. Mackey, M.C., Glass, L.: Oscillation and chaos in physiological control systems. Science **197**(4300), 287–289 (1977)
42. Marco C.: Mackey-Glass time series generator (2020). <https://www.mathworks.com/matlabcentral/fileexchange/24390-mackey-glass-time-series-generator>. Retrieved 22 Jan. MATLAB Central File Exchange
43. Lorenz, E.N.: Deterministic nonperiodic flows. J. Atmos. Sci. **20**, 130–141 (1963)
44. Alexandros L.: Chaotic Systems Toolbox (2020). <https://www.mathworks.com/matlabcentral/fileexchange/1597-chaotic-systems-toolbox>. Retrieved Jan 22. MATLAB Central File Exchange
45. Larrondo, H.: Noisefk.m (2020). <https://www.mathworks.com/matlabcentral/fileexchange/35381-noisefk-m>. Retrieved 24 Jan
46. Li, Q., Fu, Z., Yuan, N.: Beyond benford's law: distinguishing noise from chaos. PLoS ONE **10**(6), e0129,161 (2015)
47. Rosso, O.A., Olivares, F., Zunino, L., DeMicco, L., Aquino, A.L., Plastino, A., Larrondo, H.A.: Characterization of chaotic maps using the permutation bandt-pompe probability distribution. Eur. Phys. J. B **86**(4), 116 (2013)
48. Kroese, D.P., Botev, Z.I.: Spatial process generation (2013). arXiv preprint [arXiv:1308.0399](https://arxiv.org/abs/1308.0399)
49. Weisstein, E.W.: Gingerbreadman map. From MathWorld—A Wolfram web resource <http://mathworld.wolfram.com/GingerbreadmanMap.html>

Publisher's Note Springer Nature remains neutral with regard to jurisdictional claims in published maps and institutional affiliations.